Towards a More Generalized Doherty Power Amplifier Design for Broadband Operation

Towards a More Generalized Doherty Power Amplifier Design for Broadband Operation

Ayman Barakat, *Student Member, IEEE*, Mury Thian, Vincent Fusco, *Fellow*, *IEEE*, Senad Bulja, *Senior Member*, *IEEE*, and Lei Guan, *Member*, *IEEE*

***Abstract*—The conventional Doherty power amplifier (DPA) theory is limited to single carrier operations, leading to a nongeneric structure. This paper presents a new analysis that generalizes the conventional DPA theory for increased efficiency and bandwidth. We demonstrate that by introducing a theoretical parameter α at the output combiner we can redefine the relationships among the output combiner elements for a greater level of design flexibility than it was possible in the conventional DPA. We also show that previously published works in this area can be considered as special cases of the proposed general theory. As a demonstrator, a specific design, named Reduced-α Doherty power amplifier, realized using GaN HEMTs is provided to illustrate the robustness of the approach. This design proves effective for further improving the performance of the previously published 2.14/2.655 GHz dual-band parallel DPA. A maximum drain efficiency of 84% and 67% at an average of 43-dBm peak and 6-dB back-off power levels, respectively, were measured with continuous wave signals. To quantify the linearity performance, the proposed DPA was tested using wideband CDMA and long-term evolution (LTE) signals where the adjacent channel leakage ratio was recorded at –25 dBc with an average output power of 38.7 and 36.5 dBm at 2.14 and 2.655 GHz, respectively.**

***Index Terms*—Broadband, combiner, Doherty, efficiency, GaN, HEMT, load modulation, power amplifier, transmission line.**

I. Introduction

THE EVOLUTION of modern wireless communication standards from global system for mobile communications (GSM) through third-generation (3G) wideband CDMA to fourth-generation (4G) long-term evolution advanced (LTE-A) requires highly efficient RF power amplifiers (PAs) that can handle multiple frequency bands simultaneously. One of the promising candidates for this is the Doherty power amplifier (DPA) [1]–[2], which is widely favored due to its simple structure and mature implementation at GHz-frequencies.

This work was supported by the Marie Curie European Industrial Doctorate (EID) programme under the ARTISAN project (grant no. 316426).

Ayman Barakat, Mury Thian and Vincent Fusco are with the Queen's University of Belfast, ECIT Institute, Queen's Road, Queen's Island, Belfast, BT3 9DT, United Kingdom (e-mails: abarakat02@qub.ac.uk, m.thian@ecit.qub.ac.uk and v.fusco@ecit.qub.ac.uk).

Senad Bulja and Lei Guan are with Bell Laboratories, Nokia, Blanchardstown Business and Technology Park, Dublin, D15 Y6NT, Ireland (emails: senad.bulja@nokia-bell-labs.com and lei.guan@nokia-bell-labs.com).

While the conventional DPA (CDPA) [3] is effective for single frequency-band operations, it exhibits power and efficiency degradations when the operating frequency deviates from the center frequency of the output combiner. These degradations are caused by the effect of the frequency-selective quarter-wave lines (TL_1 and the output impedance transforming network (ITN) shown in Fig. 1(a)) at peak and back-off power (BOP) levels [4]–[5]. Therefore, extensive amount of research has been dedicated towards enabling the DPA for multiband operation. To achieve this goal, some publications have focused on enhancing the frequency response of the individual passive network elements using either π-networks, T-networks, single- or two-stepped ITNs [6]–[21] or microelectromechanical switches [22]–[23]. For instance, the DPA proposed in [24] has used an output matching network at the Main PA to compensate the effect of TL_1 and the output ITN. Unfortunately, such techniques result in increased complexity, larger overall physical size, and increased mismatch losses.

Other publications have recently focused on developing the output combiner of the DPA. In [4] and [25] the bandwidth of the conventional DPA is enhanced at 6-dB BOP level by reducing the transformation ratio (TR) of TL_1. However, the bandwidth was limited by the output ITN, whereas the load modulation seen by the Auxiliary PA's input impedance Z_A was not carried out properly. These drawbacks have been addressed in the 2.14/2.655-GHz dual-band parallel DPA (PDPA) [26] wherein the output ITN was omitted, and two quarter-wave lines, TL_2 and TL_3 in Fig. 1(b), were imposed to achieve proper load modulation seen by the Auxiliary PA. Consequently, the bandwidths of the output combiner at low and 6-dB BOP were improved by reducing the TR of TL_1 by a factor of two compared to that of the conventional DPA. However, two extra 35-Ω quarter-wave transmission lines, one at the Main path and one at the Auxiliary path, were required to match the 50-Ω resistance seen at the combiner's input (Z_M and Z_A in Fig. 1) at peak power (PP) to the nominal Class-E load resistance, R_{opt}, e.g. 25 Ω in [26]. Furthermore, the theoretical analysis presented in [26] cannot be directly used in the practical implementation as some tuning of the output combiner transmission line (TL) parameters are necessary, without which the high efficiency, as predicted in the theory, will not be obtained.

The same output combiner structure was adopted in [27] and [28] but with no theoretical analysis adequately provided. In

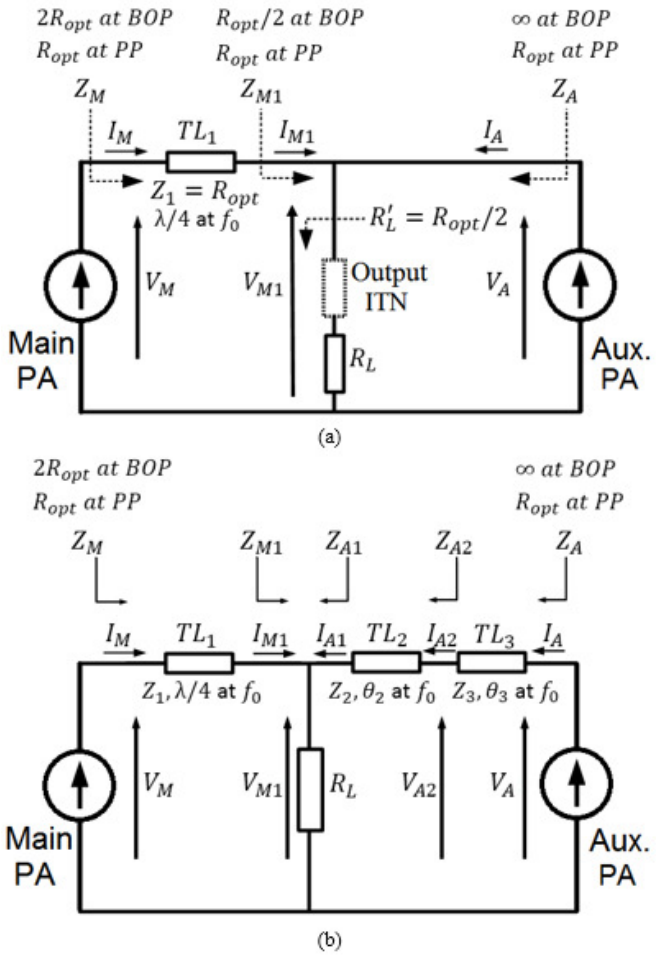

Fig. 1. Basic structures of (a) conventional Doherty power amplifier (with an output ITN), and (b) generalized Doherty power amplifier.

[29], an approach to find the exact values of this combiner parameters was presented, however, the approach provided sophisticated formulae that permitted negative characteristic impedances for TL_2 and TL_3. Moreover, other techniques have been proposed to design wideband DPAs such as digital DPA [5], three-way sequential DPA [30], and DPA with an output combiner comprised of a branch-line coupler [31].

In this paper, we propose a new analysis to provide generalized DPA theory of operation with respect to the combiner parameters. This analysis introduces, through parameter α (positive real number), simple formulae to define the relationships between the combiner parameters for a load modulation process over wide bandwidth. The new formulae provide an additional degree of design freedom through which the output ITN is no longer required. This ITN, first proposed by McMorrow [3], is typically required in the conventional DPA to transform the standard load ($R_L = 50\ \Omega$) into the combined load $R'_L = R_{opt}/2$ [4], [7]–[23], [32]–[37]. However, it occupies both Main and Auxiliary paths, leading to a reduced bandwidth and larger circuit size.

Based on this approach, a new DPA variant, named Reduced-α Doherty power amplifier (RDPA), is proposed to improve the performance of the parallel DPA and demonstrate the effectiveness of the analysis. In this design, when α is calculated, it directly reduces the structure complexity by obviating the need for the output ITN, and also by eliminating the parallel DPA's extra 35-Ω quarter-wave lines, as a result of matching Z_M and Z_A directly to R_{opt} at PP. The new design outperforms both conventional and parallel DPAs in terms of bandwidth capability at low and 6-dB BOP levels (i.e. where the Auxiliary PA is switched off). An infinite fractional bandwidth (FBW) can theoretically be achieved as a result of reducing the TR of TL_1 at 6-dB BOP by a factor of four compared to the conventional DPA.

The technical work included in this paper was partially reported in [38], whereas a complete analysis and measurements are given in this paper. This paper is organized as follows. Section II presents the derivation of the new analysis along with the resulting design formulae and operational conditions. Section III explains the design procedures of the proposed Reduced-α DPA combiner, followed by a comparison of its simulated performance with that of the parallel DPA in Section IV. Section V describes implementation and measurement of the Reduced-α DPA with continuous wave (CW) signals. In Section VI, the linearity performance of the realized DPA is examined through modulated signal measurements. Finally, the conclusions of this paper are given in Section VII.

II. Basic Operation and Analysis of the Generalized Doherty Power Amplifier

The basic structures of the conventional and generalized DPAs are illustrated in Fig. 1. In the conventional DPA, an output ITN is required to transform $R_{opt}/2$ to the standard 50-Ω load impedance whereas in the generalized DPA two transmission lines TL_2 and TL_3 are inserted at the Auxiliary PA output. The three lines TL_1, TL_2 and TL_3 are quarter-wave lines at the center angular frequency (ω_0). Therefore, to ensure the phase of the signal in the Main PA path match the phase of the signal in the Auxiliary PA path prior to them being combined, a 90° delay transmission line, not shown in Fig. 1, needs to be added at the input of the Auxiliary PA (for the case of the conventional DPA) or at the input of the Main PA (for the case of the generalized DPA). The analysis of the generalized DPA presented below is based upon assumptions that both Main and Auxiliary PAs are operated in Class-B mode, and that their output currents and voltages follow the ideal characteristics shown in Fig. 2.

Phasors of the fundamental output currents of the Main and Auxiliary PAs, denoted here respectively as $\vec{I}_M$ and $\vec{I}_A$, can be described as follows [2]:

$$\vec{I}_M = \frac{I_{max}}{4}(1+\xi)\ e^{j(\omega_0 t+\vartheta_M)}, \tag{1}$$

$$\vec{I}_A = \frac{I_{max}}{2}\xi\ e^{j(\omega_0 t+\vartheta_A)} = \frac{I_{max}}{2}\xi\ e^{j(\omega_0 t+\vartheta_M+\pi/2)}, \tag{2}$$

where parameter ξ varies from 0 to 1 as the input drive voltage (v_{in}) increases from $V_{max}/2$ to V_{max}, I_{max} is the maximum amplitude of the output RF current, ϑ_M and ϑ_A are the phase shift angles of $\vec{I}_M$ and $\vec{I}_A$ respectively. Let us consider now Fig. 1(b), the impedances seen by TL_1, i.e., Z_{M1} and by TL_2, i.e., Z_{A1} are:

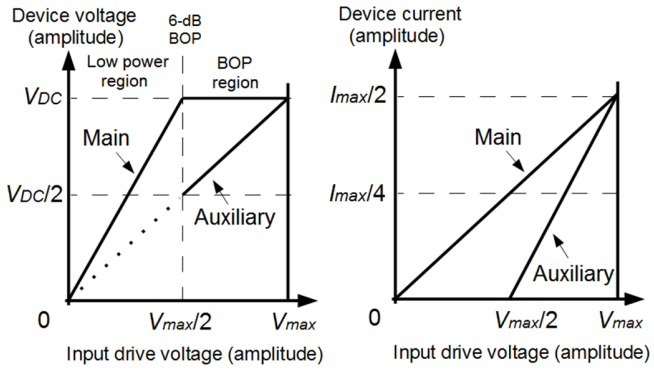

Fig. 2. Idealized characteristics of fundamental output voltages and currents of the Main and Auxiliary PAs operated in Class-B mode.

$$Z_{M1} = R_L\left(1 + \frac{\vec{I}_{A1}}{\vec{I}_{M1}}\right) = R_L\left(1 + \frac{I_{A1}}{I_{M1}}\right), \tag{3}$$

$$Z_{A1} = R_L\left(1 + \frac{\vec{I}_{M1}}{\vec{I}_{A1}}\right) = R_L\left(1 + \frac{I_{M1}}{I_{A1}}\right), \tag{4}$$

where $\vec{I}_{M1}$ and $\vec{I}_{A1}$ are always in phase.

A. *Main PA branch*

The relationships between input and output voltages as well as input and output currents of TL_1 can be described using the ABCD matrix definition for TL_1 as follows:

$$\begin{bmatrix}\vec{V}_M \\ \vec{I}_M\end{bmatrix} = \begin{bmatrix}0 & jZ_1 \\ jY_1 & 0\end{bmatrix}\begin{bmatrix}\vec{V}_{M1} \\ \vec{I}_{M1}\end{bmatrix}, \tag{5}$$

$$\vec{V}_M = jZ_1\vec{I}_{M1}, \tag{6}$$

$$\vec{I}_M = jY_1\vec{V}_{M1}. \tag{7}$$

From (6) $\vec{I}_{M1}$ is given as

$$\vec{I}_{M1} = -j\frac{\vec{V}_M}{Z_1}. \tag{8}$$

Now we need to derive an expression for $\vec{I}_{A1}$ in terms of $\vec{I}_A$, Z_2, and Z_3. This can be obtained using the ABCD matrix definition for TL_2 and TL_3 as follows:

$$\begin{bmatrix}\vec{V}_{A2} \\ \vec{I}_{A2}\end{bmatrix} = \begin{bmatrix}0 & jZ_2 \\ jY_2 & 0\end{bmatrix}\begin{bmatrix}\vec{V}_{M1} \\ \vec{I}_{A1}\end{bmatrix}, \tag{9}$$

$$\begin{bmatrix}\vec{V}_A \\ \vec{I}_A\end{bmatrix} = \begin{bmatrix}0 & jZ_3 \\ jY_3 & 0\end{bmatrix}\begin{bmatrix}\vec{V}_{A2} \\ \vec{I}_{A2}\end{bmatrix}. \tag{10}$$

From (9) we can extract the following relation

$$\vec{V}_{A2} = jZ_2\vec{I}_{A1}. \tag{11}$$

From (10) we can obtain

$$\vec{I}_A = jY_3\vec{V}_{A2}. \tag{12}$$

From (11) and (12) we can express $\vec{I}_{A1}$ as follows:

$$\vec{I}_{A1} = -\frac{Z_3}{Z_2}\vec{I}_A. \tag{13}$$

By substituting (8) and (13) into (3), Z_M can be obtained from the quarter-wave impedance transformation formula as follows:

$$Z_M = \frac{Z_1^2}{Z_{M1}} = \frac{Z_1^2}{R_L\left(1 - j\frac{Z_1Z_3\vec{I}_A}{Z_2\vec{V}_M}\right)}. \tag{14}$$

Hence, the fundamental output voltage of the Main PA is

$$\vec{V}_M = \vec{I}_M Z_M = \frac{\vec{I}_M Z_1^2}{R_L\left(1 - j\frac{Z_1Z_3\vec{I}_A}{Z_2\vec{V}_M}\right)}. \tag{15}$$

Next we substitute $\vec{I}_M$ and $\vec{I}_A$ described in (1) and (2) into (15) to obtain the following relation:

$$\vec{V}_M = \frac{\frac{I_{max}}{4}(1+\xi)\ e^{j(\omega_0 t+\vartheta_M)}Z_1^2}{R_L\left(1 - j\frac{Z_1Z_3\frac{I_{max}}{2}\xi\ e^{j(\omega_0 t+\vartheta_M+\pi/2)}}{Z_2\vec{V}_M}\right)}. \tag{16}$$

After re-arranging (16), $\vec{V}_M$ can be expressed as

$$\vec{V}_M = Z_1\left(\frac{I_{max}}{2}\right)\left\{\frac{Z_1}{2R_L} + \xi\left(\frac{Z_1}{2R_L} - \frac{Z_3}{Z_2}\right)\right\}e^{j(\omega_0 t+\vartheta_M)}. \tag{17}$$

From Fig. 2, it can be observed that the voltage amplitude V_M is constant (i.e. equal to V_{dc}) for input drive ranging from $V_{max}/2$ to V_{max}. To accomplish this, $\vec{V}_M$ in (17) must be set independent of ξ, resulting in (18) and (19). For the convenience of subsequent analysis, a *new parameter* α is introduced.

$$\frac{Z_1}{2R_L} = \frac{Z_3}{Z_2} = \alpha \tag{18}$$

$$V_M = \left(\frac{I_{max}}{2}\right)\left(\frac{Z_1^2}{2R_L}\right) = V_{dc} \tag{19}$$

To achieve maximum output voltage swing of V_{dc} in Class-B mode, the fundamental impedance seen by the PA must be equal to

$$R_{opt} = V_{dc}\left(\frac{2}{I_{max}}\right). \tag{20}$$

Given (20) and from the inspection of Fig. 2, we can calculate Z_M at 6-dB BOP level, i.e., at $v_{in} = V_{max}/2$ and at PP level, i.e., at $v_{in} = V_{max}$ as given below:

$$Z_{M_{BOP}} = \frac{V_M}{I_M} = \frac{V_{dc}}{\frac{I_{max}}{4}} = 2R_{opt}, \tag{21}$$

$$Z_{M_{PP}} = \frac{V_M}{I_M} = \frac{V_{dc}}{\frac{I_{max}}{2}} = R_{opt}. \tag{22}$$

Further from (19) and (20), we obtain

$$\frac{Z_1^2}{2R_L} = R_{opt}. \tag{23}$$

Subsequently, the characteristic impedance of TL_1 (Z_1) and the load impedance (R_L) can be calculated from (18) and (23) as follows:

$$Z_1 = \frac{R_{opt}}{\alpha}, \tag{24}$$

$$R_L = \frac{R_{opt}}{2\alpha^2}. \tag{25}$$

In the conventional DPA, an output ITN is typically needed to transform $R_L' = R_{opt}/2$ into $R_L = 50\,\Omega$. For single band operation, a single-stepped ITN is often sufficient whereas for broadband operation a more sophisticated two- or three-stepped ITN needs to be employed, resulting in increased circuit complexity and large physical size. In the generalized DPA, the degree of design freedom is increased by one through the introduction of parameter α, which might dispense with the need for the output ITN.

The impedance Z_M described in (21) – (22) is transformed by TL_1 into the following impedance:

$$Z_{M1_{BOP}} = \frac{Z_1^2}{Z_{M\_BOP}} = \frac{\left(\frac{R_{opt}}{\alpha}\right)^2}{2R_{opt}} = \frac{R_{opt}}{2\alpha^2} = R_L, \tag{26}$$

$$Z_{M1_{PP}} = \frac{Z_1^2}{Z_{M\_PP}} = \frac{\left(\frac{R_{opt}}{\alpha}\right)^2}{R_{opt}} = \frac{R_{opt}}{\alpha^2} = 2R_L. \tag{27}$$

As can be seen from Fig. 1, the only bandwidth-limiting element in the Main PA branch is TL_1. Using (21), (22), (26), and (27) we can describe the FBW of TL_1 at PP and BOP as follows [39]:

$$\mathrm{FBW_{TL1}} = \left|2 - \frac{4}{\pi} cos^{-1}\left(\frac{\Gamma_m}{\sqrt{1-\Gamma_m{}^2}}\gamma(\alpha)\right)\right|, \tag{28}$$

where Γ_m is the maximum reflection coefficient magnitude can be tolerated at the combiner input within the bandwidth of interest (assuming $\Gamma(\omega_0) = 0$ at both PP and 6-dB BOP), and $\gamma(\alpha)$ is a parameter that depends on α and the power level which can be expressed as

$$\gamma(\alpha) = \begin{cases} \dfrac{2\alpha}{|1-\alpha^2|}, & \text{at peak power,} \\ \dfrac{4\alpha}{|1-4\alpha^2|}, & \text{at } 6-\text{dB BOP.} \end{cases} \tag{29}$$

For instance, if the minimum tolerable input return loss of TL_1 is assumed to be 10 dB then using (28) we can plot $\mathrm{FBW_{TL1}}$ as a function of α as shown in Fig. 3. This figure implies the bandwidth capabilities of the generalized DPA at PP and 6-dB BOP levels. Clearly, for $\alpha = 0.5$, termed here as Reduced-α DPA, $\mathrm{FBW_{TL1}}$ is infinity at BOP which means the combiner response is independent of frequency, and $Z_{M_{BOP}} = 2R_{opt}$ over the entire spectrum. Notice that this feature of the Reduced-α DPA combiner would not change even if the threshold Γ_m is reduced to zero. The figure also shows the bandwidth capabilities at $\alpha = 1$, which corresponds to the conventional DPA [1], and at $\alpha = 1/\sqrt{2}$, which corresponds to the ideal case of the parallel DPA (i.e., without the extra 35-Ω lines).

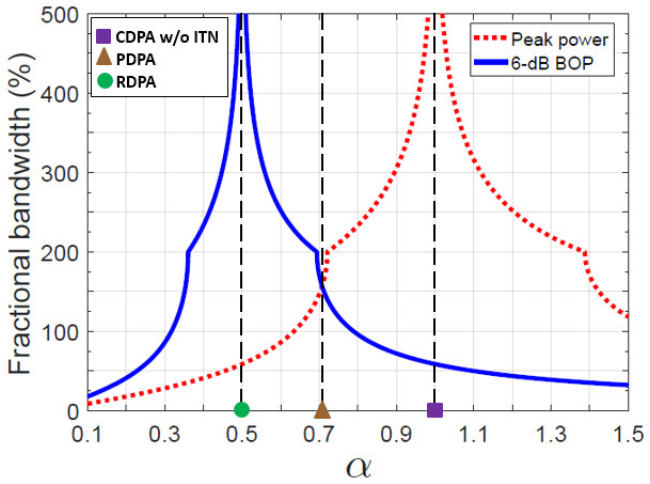

Fig. 3. Fractional bandwidth of TL_1 as a function of α at PP and 6-dB BOP levels (corresponds to a minimum return loss of 10 dB).

B. Auxiliary PA branch

At 6-dB BOP level, the Main PA is ON while the Auxiliary PA is OFF. Since the output current of the Auxiliary PA is zero, the impedance Z_A is infinity, (30). Subsequently, TL_2 and TL_3 will transform this impedance into an open circuit at the center frequency, and provide good isolation over a wide bandwidth.

$$Z_{A_{BOP}} = Z_{A1_{BOP}} = \infty \tag{30}$$

At PP level, both Main and Auxiliary PAs are ON. From the inspection of Fig. 2, we can calculate

$$Z_{A_{PP}} = \frac{V_A}{I_A} = \frac{V_{dc}}{\frac{I_{max}}{2}} = R_{opt}, \tag{31}$$

where R_{opt} is defined in (20). Further, the impedance Z_{A1} can be determined as follows:

$$Z_{A1_{PP}} = \frac{Z_2^2}{Z_{A2_{PP}}} = \frac{Z_2^2}{\frac{Z_3^2}{Z_{A_{PP}}}} = R_{opt}\left(\frac{Z_2}{Z_3}\right)^2 = \frac{R_{opt}}{\alpha^2} = 2R_L. \tag{32}$$

The foregoing analysis assumes that the electrical lengths of TL_2 and TL_3 (i.e., θ_2 and θ_3) are fixed, i.e., 90°, and the corresponding basic circuit schematic is depicted in Fig. 4 with component values given in terms of α and R_{opt} based upon the calculations in (21)–(22), (26)–(27), and (30)–(32). In the following analysis, the frequency behavior of the proposed generalized DPA is examined, i.e., this is the case when the carrier frequency (f_c) is varied apart from the center frequency (f_0). Since the physical lengths of TL_2 and TL_3 are constant, then θ_2 and θ_3 will also vary as follows:

$$\theta_2 = \theta_3 = \theta = \frac{\pi}{2}\frac{f_c}{f_0} = \frac{\pi}{2}k, \tag{33}$$

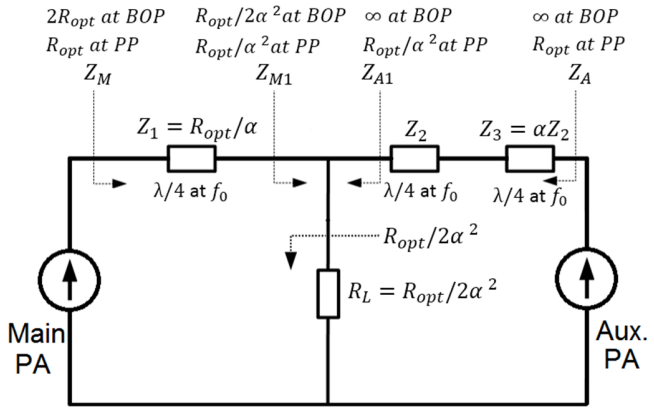

Fig. 4. Basic circuit schematic of the generalized DPA.

where k is the normalized frequency. The values of Z_{A2} and Z_A at PP level can be computed using lossless transmission line formula as follows:

$$Z_{A2_{PP}} = Z_2 \frac{Z_{A1_{PP}} + jZ_2 tan\theta}{Z_2 + jZ_{A1_{PP}} tan\theta}, \tag{34}$$

$$Z_{A_{PP}} = Z_3 \frac{Z_{A2_{PP}} + jZ_3 tan\theta}{Z_3 + jZ_{A2_{PP}} tan\theta}. \tag{35}$$

where $Z_{A1_{PP}}$ is given in (32) and the relationship between Z_2 and Z_3 is described in (18). Substituting (34) into (35) yields:

$$Z_{A_{PP}} = \alpha Z_2 \frac{2R_L(1 - \alpha tan^2\theta) + jZ_2(1+\alpha)tan\theta}{Z_2(\alpha - tan^2\theta) + j2R_L(1+\alpha)tan\theta}. \tag{36}$$

The magnitude of $Z_{A_{PP}}$ and its normalized magnitude are expressed as follows:

$$|Z_{A_{PP}}| = \alpha Z_2 \sqrt{\frac{4R_L^2(1 - \alpha tan^2\theta)^2 + Z_2^2(1+\alpha)^2 tan^2\theta}{Z_2^2(\alpha - tan^2\theta)^2 + 4R_L^2(1+\alpha)^2 tan^2\theta}}, \tag{37}$$

$$\frac{|Z_{A_{PP}}|}{R_{opt}} = \frac{\sqrt{\dfrac{\left(\frac{2R_L}{Z_2}\right)^2 \left\{1 - \alpha tan^2\left(\frac{k\pi}{2}\right)\right\}^2 + (1+\alpha)^2 tan^2\left(\frac{k\pi}{2}\right)}{\left\{\alpha - tan^2\left(\frac{k\pi}{2}\right)\right\}^2 + \left(\frac{2R_L}{Z_2}\right)^2 (1+\alpha)^2 tan^2\left(\frac{k\pi}{2}\right)}}}{\alpha\left(\frac{2R_L}{Z_2}\right)}, \tag{38}$$

where R_{opt} is given in (25). Notice from (36) that for $\theta = 90°$, $Z_{A_{PP}}$ will no longer depend on Z_2. Illustrated in Fig. 5 is the frequency response of $Z_{A_{PP}}$ for different values of Z_2 where α and R_L are fixed, i.e., α = 0.5 and R_L = 50 Ω. Here Z_2 controls the bandwidth of the Auxiliary branch.

C. *Power and efficiency of the generalized DPA versus bandwidth*

The generalized DPA output power at 6-dB BOP level can be derived as follows:

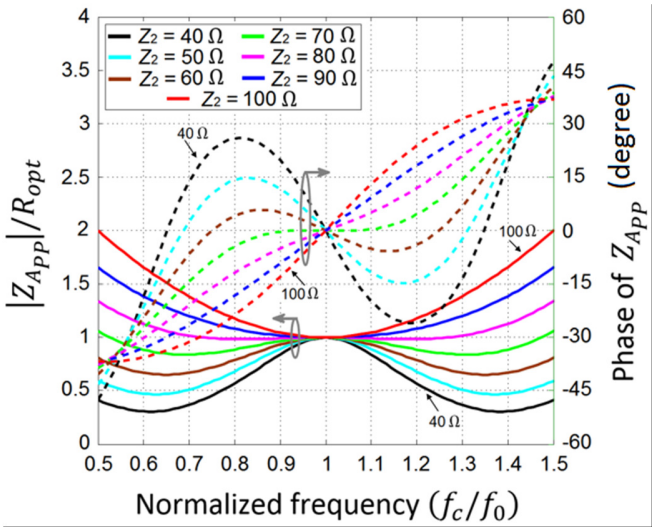

Fig. 5. Frequency response of $Z_{A_{PP}}$ for different values of Z_2. Note $\alpha = 0.5$ and $R_L = 50$ Ω.

$$P_{out_{BOP}} = \frac{1}{2} I_M V_M \cos\varphi_{M_{BOP}} = \frac{1}{2}\frac{I_{max}}{4} V_{dc} \cos\varphi_{M_{BOP}} = \frac{1}{4} P_{out_{max}} \cos\varphi_{M_{BOP}}, \tag{39}$$

where $P_{out_{max}}$ is the maximum DPA output power at f_0, and

$$\cos\varphi_{M_{BOP}} = \frac{\text{real}\{Z_{M_{BOP}}(\theta)\}}{|Z_{M_{BOP}}(\theta)|}. \tag{40}$$

Here $Z_{M_{BOP}}(\theta)$ is obtained by substituting (24) and (26) in the lossless transmission line equation of TL_1 at 6-dB BOP resulting in

$$Z_{M_{BOP}}(\theta) = \frac{R_{opt}}{\alpha} \frac{1 + j\,2\,\alpha \tan\theta}{2\,\alpha + j \tan\theta}. \tag{41}$$

Having known the DPA dc power formulae from [2], the drain efficiency (DE) at 6-dB BOP can be written as

$$\eta_{6dB} = \frac{\pi}{4} \cos\varphi_{M_{BOP}}. \tag{42}$$

At PP operation the output power of the generalized DPA can be derived as follows:

$$P_{out_{PP}} = \frac{1}{2} I_M V_M \cos\varphi_{M_{PP}} + \frac{1}{2} I_A V_A \cos\varphi_{A_{PP}} = \frac{1}{2}\frac{I_{max}}{2} V_{dc}\left(\cos\varphi_{M_{PP}} + \cos\varphi_{A_{PP}}\right) = \frac{1}{2} P_{out_{max}}\left(\cos\varphi_{M_{PP}} + \cos\varphi_{A_{PP}}\right), \tag{43}$$

where

$$\cos\varphi_{M_{PP}} = \frac{\text{real}\{Z_{M_{PP}}(\theta)\}}{|Z_{M_{PP}}(\theta)|}, \tag{44}$$

$$\cos\varphi_{A_{PP}} = \frac{\text{real}\{Z_{A_{PP}}(\theta)\}}{|Z_{A_{PP}}(\theta)|}, \tag{45}$$

and $Z_{M_{PP}}(\theta)$ is obtained by substituting (24) and (27) in the lossless transmission line equation of TL_1 at PP resulting in

$$Z_{M_{PP}}(\theta) = \frac{R_{opt}}{\alpha}\,\frac{1 + j\,\alpha \tan\theta}{\alpha + j\tan\theta}. \tag{46}$$

By substituting (25), and $Z_2 = \frac{R_{opt}}{\alpha^{3/2}}$ in (36), $Z_{A_{PP}}$ can be described as

$$Z_{A_{PP}}(\theta) = \frac{R_{opt}}{\sqrt{\alpha}}\left[\frac{(1 - \alpha tan^2\theta) + j\sqrt{\alpha}(1+\alpha)tan\theta}{\sqrt{\alpha}(\alpha - tan^2\theta) + j(1+\alpha)tan\theta}\right]. \tag{47}$$

For a maximum dc power equals to $2(I_{max}/\pi)V_{dc}$, the DE at PP can be written as

$$\eta_{PP} = \frac{\pi}{4}\frac{1}{2}\left(\cos\varphi_{M_{PP}} + \cos\varphi_{A_{PP}}\right). \tag{48}$$

Note that Z_2 in (36) can be selected arbitrarily, but here we have chosen its optimum definition, i.e., (49), over 25% FBW as will be demonstrated in Section III.

The output power and efficiency of the generalized DPA are plotted against k for different values of α as depicted in Figs. 6 and 7. From these figures we observe that the generalized DPA provides an ideal Performance at f_0 regardless of the value of α. As f_c deviates from f_0 the parameter α takes control of the power and efficiency degradations. The effect of α here confirms the results observed in Fig. 3 where best performance at BOP and PP corresponds to $\alpha = 0.5$ and $\alpha = 1$, respectively. For instance, with $\alpha = 0.5$ the back-off efficiency is 1.25 times higher than that of the conventional DPA [1] at $k = 0.5$.

To conclude, the Reduced-α DPA is analytically able to eliminate any bandwidth limitations caused by the combiner at low and 6-dB BOP operation. Whereas its relatively moderate performance at PP might be enhanced, for example, by means of enabling the Auxiliary PA to provide higher power and efficiency at PP through unsymmetrical DPA designs [4]. Note that the conventional DPA [3] has proven power and efficiency degradations with respect to the FBW not only at BOP but also at PP, as reported in [4], due to the imposed output ITN.

III. Reduced-α DPA Design Procedure

An example with step-by-step design procedures is given below to elucidate the basic operation and theory of the proposed generalized DPA described in Section II. The generalized DPA is designed to operate within 2.1–2.7 GHz frequency range, i.e., 25% FBW. The broadband Class-E PA [40]–[42] employing reactance compensation technique with a nominal resistance (R_{opt}) of 25 Ω reported in [26] is used as Main and Auxiliary PAs. The generalized DPA is terminated with standard 50 Ω load resistance (R_L).

Step 1: Calculate α using (25)

$$\alpha = \sqrt{R_{opt}/2R_L} = \sqrt{25/100} = 0.5$$

This step avoids imposing either an output ITN or any extra quarter-wave lines. Furthermore, this value of α flattens the frequency response of the combiner, over the entire spectrum, at 6-dB BOP level and below. Note that if R_{opt} was not predetermined, then (25) would be used to calculate R_{opt} required for the PA cell based on the desired value of α.

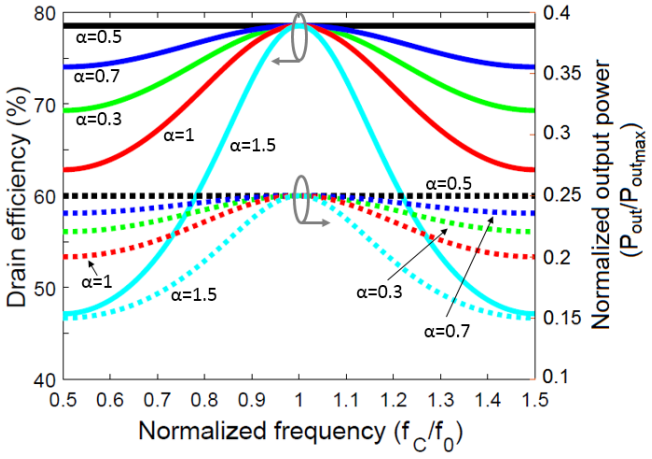

Fig. 6. Output power and efficiency of the generalized DPA at 6-dB BOP for $\alpha = 0.3, 0.5, 1/\sqrt{2}, 1,$ and 1.5.

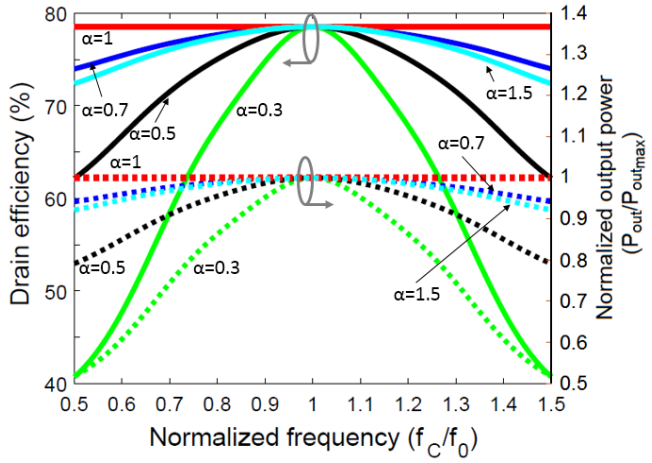

Fig. 7. Output power and efficiency of the generalized DPA at PP for $\alpha = 0.3, 0.5, 1/\sqrt{2}, 1,$ and 1.5.

Step 2: Calculate Z_1 using (24)

$$Z_1 = \frac{R_{opt}}{\alpha} = 50\ \Omega$$

Step 3: Determine Z_2 and Z_3

Given R_L and α, the optimum value of Z_2 can be obtained graphically as follows:

(i) Using (36) and (38) respectively, plot the phase and the normalized amplitude of $Z_{A_{PP}}$ for different values of Z_2.

(ii) From these two plots, determine Z_2 that gives minimal amplitude and phase variation over the required FBW.

From Fig. 5, the optimum Z_2 is 70 Ω since this value gives minimal phase variation <0.9° and minimal amplitude variation <5.4% across 25% FBW. Alternatively, by assuming $Z_{A2_{PP}} = R_{opt}/\alpha$, the optimum Z_2 can be calculated from (49) which gives a more accurate result than the one obtained from the graphical representation, which relies on the resolution of the sweeping intervals (10 Ω).

$$Z_2 = \frac{R_{opt}}{\alpha^{3/2}} = 70.71\ \Omega \qquad (49)$$

Subsequently, the value of Z_3 can be calculated using (18) as follows:

$$Z_3 = \alpha\, Z_2 = \frac{R_{opt}}{\alpha^{1/2}} = 35.36\ \Omega.$$

As can be seen from Fig. 8, Z_A has now been optimally matched to the PA cell nominal resistance ($R_{opt} = 25\ \Omega$) at PP level over the required bandwidth, and compared with the parallel DPA, the proposed Reduced-α DPA offers better matching within 25% FBW. The final circuit schematic of the proposed Reduced-α DPA is illustrated in Fig. 9. Table I shows a comparison between different DPA topologies, from which it can be seen that for $\alpha = 1/\sqrt{2}$ the generalized DPA is reduced to the parallel DPA and for $\alpha = 1$ the generalized DPA is reduced to the conventional DPA, implying that parallel DPA and conventional DPA are essentially a subset of the generalized DPA. In addition, it is observed that the DPA designs reported in [27], [29] and [28] have α=0.6, 0.6 and 0.4, respectively. Hence, the method presented in this paper helps classifying various DPA topologies.

The frequency response of the impedances $Z_{M_{BOP}}$, $Z_{M_{PP}}$, and $Z_{A_{PP}}$ is examined for the conventional, parallel, and Reduced-α DPAs. For the conventional DPA, a two-stepped output ITN is inserted to provide a dual-band behavior. At 6-dB BOP the Reduced-α DPA outperforms the other DPAs and achieves an ideal behavior over the entire indicated frequency range as shown in Figs. 10(a) and (b). At PP level, the impedance $Z_{A_{PP}}$ has almost the same behavior for the conventional and Reduced-α DPAs as depicted in Fig. 10(c) and (d). Meanwhile, at the Main side, $Z_{M_{PP}}$ for the conventional DPA has the best response for up to 40% FBW, while all topologies exhibit poor response at higher FBW as shown in Figs. 10 (e) and (f).

IV. Circuit Simulation

The circuit schematic of the Reduced-α DPA used in the simulations is depicted in Fig. 11. The substrate used was Rogers RO4350B model with 0.508-mm thickness, a dielectric constant of 3.66, and a loss tangent of 0.0037. Two 10-W GaN HEMTs CGH40010F from Cree were used to deliver a total PP of 43 dBm. A 90° hybrid coupler 11306-3S from Anaren was used to split the input power equally and provide 90° phase shift at the input of the Main PA. The Class-E circuit reported in [26] was used as the Main and Auxiliary PAs. The structure of the output combiner is based on Fig. 9 with $\alpha = 0.5$. The electrical lengths of the 25-Ω offset lines were optimized for better isolation and efficiency. Table II shows theoretical and actual values of the output combiner parameters. No tuning was performed in the Reduced-α DPA simulation as opposed to the parallel DPA, leading to a consistency between theory and realization. The gate bias voltages of the Main and Auxiliary PAs were set to $V_{gM} = -3.15$ V and $V_{gA} = -7$ V, respectively, and the drain voltage of both cells was kept at $V_{dc} = 28$ V.

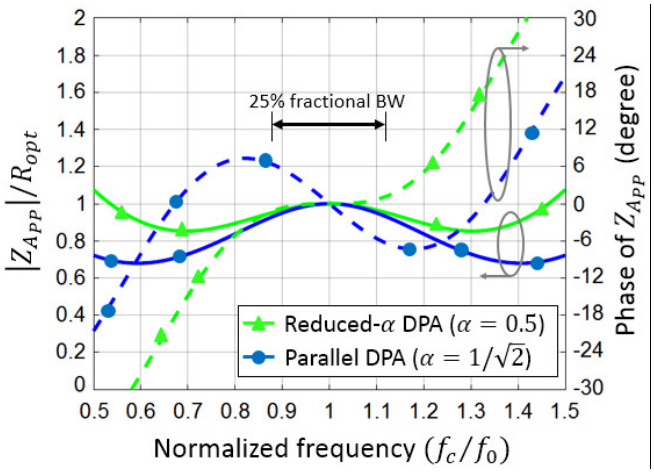

Fig. 8. Theoretical magnitude (solid lines) and phase (dashed lines) of $Z_{A_{PP}}$ for the parallel and proposed Reduced-α DPA.

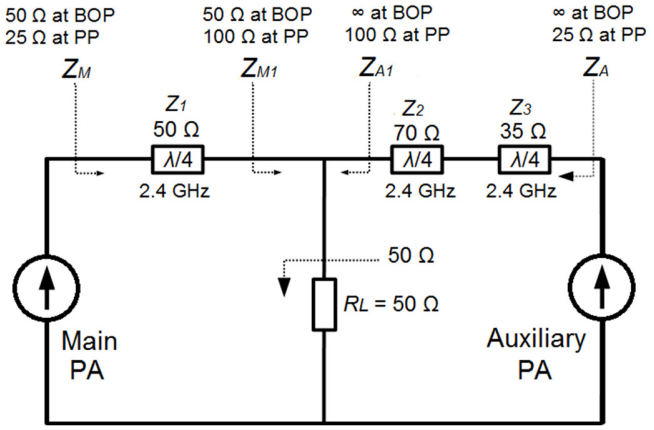

Fig. 9. Circuit schematic of the 2.1–2.7 GHz Reduced-α DPA.

TABLE I
Output Combiner Parameters

	GDPA	RDPA	PDPA	CDPA
$\boldsymbol{\alpha}$	$0 < \alpha < \infty$	0.5	$\frac{1}{\sqrt{2}}$	1
$\boldsymbol{Z_1}$	$\frac{R_{opt}}{\alpha}$	$2R_{opt}$	$\sqrt{2}R_{opt}$	R_{opt}
$\boldsymbol{R_L}$	$\frac{R_{opt}}{2\alpha^2}$	$2R_{opt}$	R_{opt}	$\frac{R_{opt}}{2}$
$\frac{\boldsymbol{Z_3}}{\boldsymbol{Z_2}}$	α	0.5	$\frac{1}{\sqrt{2}}$	-

A. Small signal performance

Fig. 12 shows a comparison of the simulated $|S_{11}|$ and $|S_{21}|$ of the Reduced-α DPA with the parallel DPA. Input return loss and small-signal gain were better than 11.5 dB and 10.5 dB, respectively, across a frequency range from 2.1 to 2.7 GHz (25% FBW).

B. Large signal performance

Fig. 13 shows the simulated output power and DE versus frequency at 36-dBm input power (corresponding to the PP

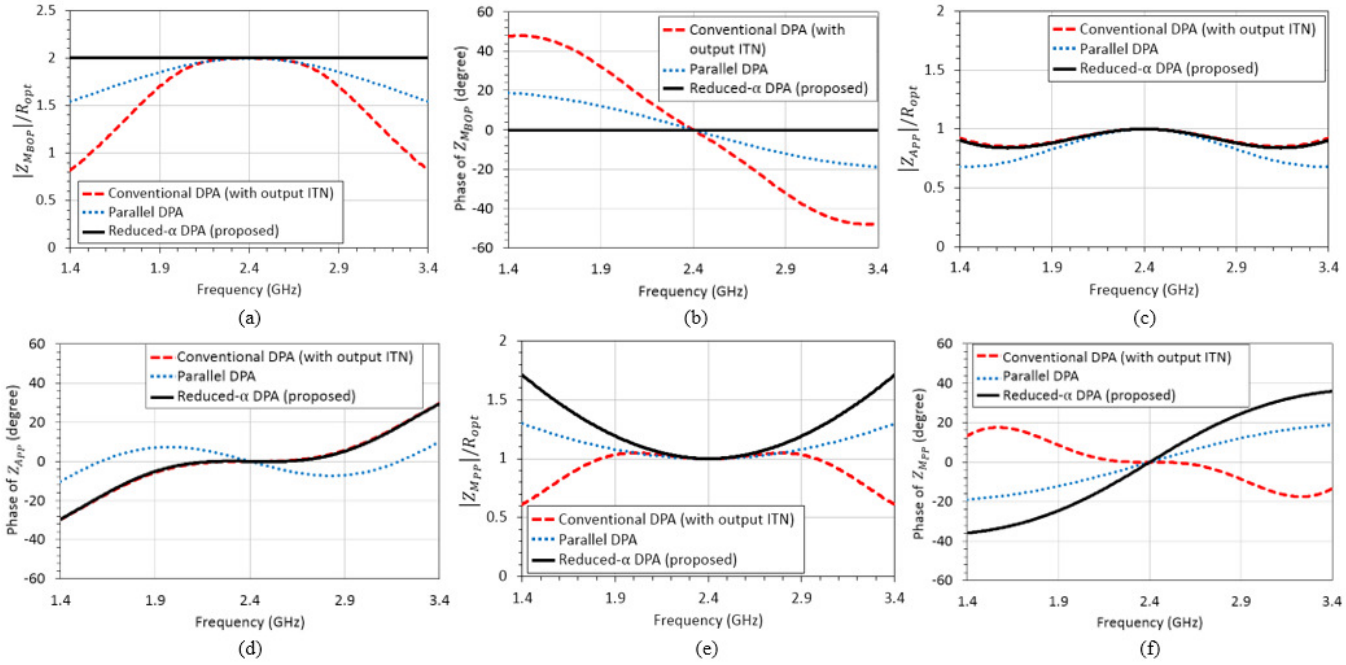

Fig. 10 Simulated Main and Auxiliary impedances against frequency for the output combiner of the conventional, parallel and Reduced-α DPAs: (a) Normalized magnitude of Main impedance at 6-dB BOP. (b) Phase of Main impedance at 6-dB BOP. (c) Normalized magnitude of Auxiliary impedance at PP. (d) Phase of Auxiliary impedance at PP. (e) Normalized magnitude of Main impedance at PP. (f) Phase of Main impedance at PP.

level). A significant DE improvement, up to 9.1 points (from 67.2% to 76.3% at 2.65 GHz), is observed over a FBW of 25%, with a maximum value of 81.6% achieved at 2.18 GHz. The output power is maintained at around 43 dBm over the intended bandwidth.

Fig. 14 shows the simulated output power and DE versus frequency at 27.5-dBm input power (corresponding to the BOP level). Similarly, the DE has improved up to 14 points (from 51.5% to 65.5% at 2.4 GHz) over the 2.1–2.7 GHz frequency range where the output power was hovering around 37.5 dBm. The maximum DE observed was 66.4% at 2.28 GHz.

Figs. 15 and 16 show the simulated gain and DE versus output power at 2.14 GHz (center frequency of the lower band 2.11–2.17 GHz) and at 2.655 GHz (center frequency of the upper band 2.62–2.69 GHz), respectively, with input power swept from 0 to 36 dBm. For the lower band, the DE reached a maximum of 81.4% at 42.8 dBm and 54.4% at 6-dB output BOP level. For the upper band, the DE reached a maximum of 76.6% at 43.3 dBm and 62.1% at 6-dB output BOP. The fundamental drain currents of the Main and Auxiliary PAs at 2.14 and 2.655 GHz are shown in Figs. 17 and 18. A current ratio 1:1 is obtained at PP level, conforming to the theory in Section II.

V. Implementation and CW Measurements

The Reduced-α DPA was realized on Rogers RO4350B substrate which was used in the simulations. Fig. 19 shows the fabricated DPA prototype with a total size of 10 cm × 6.2 cm. CW measurements were carried out using Rohde & Schwarz SMW200A signal generator and FSUP spectrum analyzer. A driver amplifier RUP15020-11 from RFHIC was used to boost the input power fed to the DPA up to 36 dBm. A 30-dB attenuator was inserted at the output of the DPA to protect the spectrum analyzer. Three 32V/10A dc power supplies were used to supply the required gate and drain bias voltages for both the driver and the DPA.

TABLE II
Theoretical and Actual Output Combiner Parameter Values of the Parallel and Reduced-α DPAs

Parameter	Parallel DPA		Reduced-α DPA	
	Theory	Actual	Theory	Actual
Z_1	70.7 Ω	60.7 Ω	50 Ω	50 Ω
θ_1 @ 2.4 GHz	90°	72.9°	90°	90°
Z_2	70.7 Ω	60.7 Ω	70.7 Ω	70.7 Ω
θ_2 @ 2.4 GHz	90°	72.9°	90°	90°
Z_3	50 Ω	49.6 Ω	35.4 Ω	35.4 Ω
θ_3 @ 2.4 GHz	90°	88°	90°	90°

Fig. 20 shows the measured S-parameters, obtained with gate bias voltages optimized to $V_{gM} = -2.7$ V and $V_{gA} = -4.75$ V while the drain voltage is maintained at 28 V. Input return loss was better than 8 dB from 2 to 2.9 GHz, and better than 10 dB at the lower and upper band frequencies. The small-signal gain in the lower frequency band was higher than that in the upper frequency band. This is consistent with the fact that the output return loss is better in the lower frequency band. Measured output power, gain and DE at PP level are plotted in Fig. 21 against frequency. A maximum DE of 83.7% is obtained at 2.34 GHz. The PA exhibits DE ≥ 65% within 500-MHz frequency range from 2.1 to 2.6 GHz. The PA delivered 43 ± 2 dBm saturated output power within the required bandwidth. Shown in Fig. 22 is the PA performance at 6 dB BOP level. A maximum DE of 66.8% was recorded at 2.2 GHz. The DE was ≥ 50% within 420-MHz bandwidth from 2.1 to 2.52 GHz.

Fig. 23 shows the measured gain and DE against output

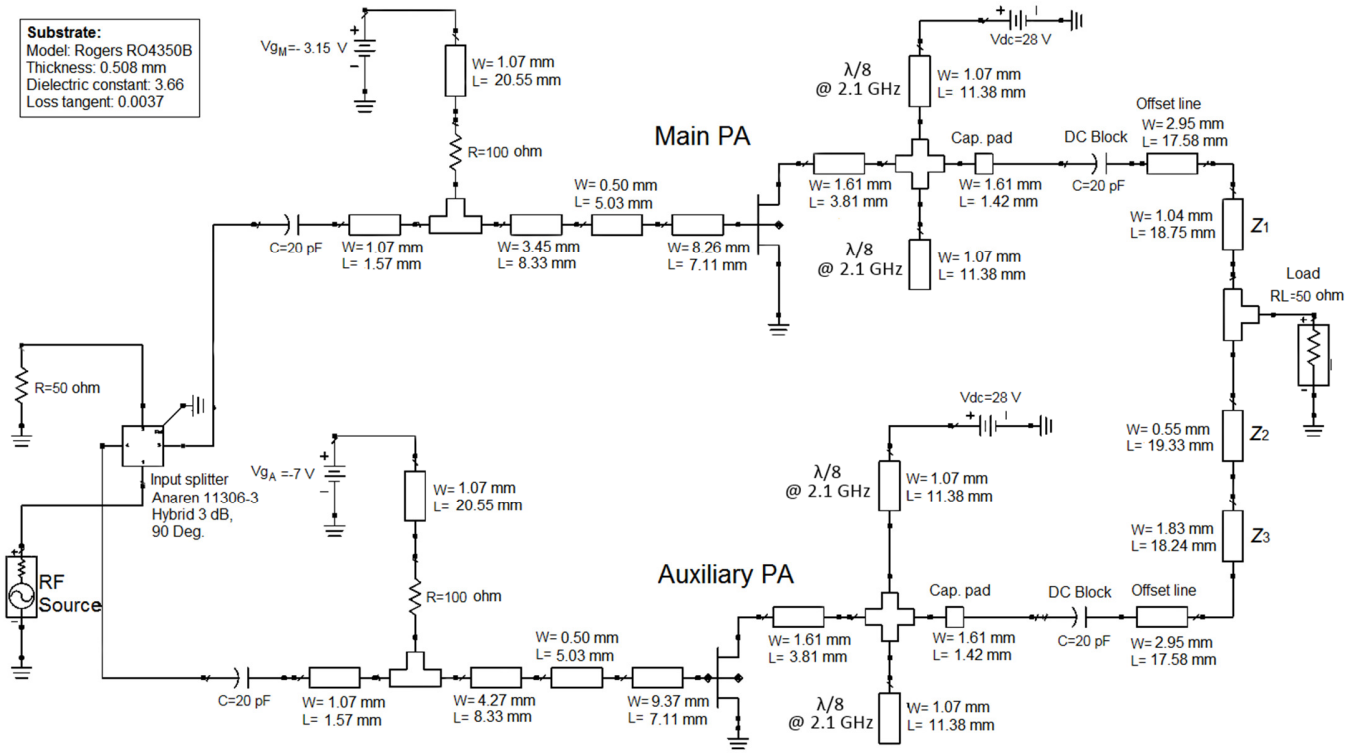

Fig. 11. Simulated circuit schematic of the proposed 2.1–2.7 GHz Reduced-α DPA.

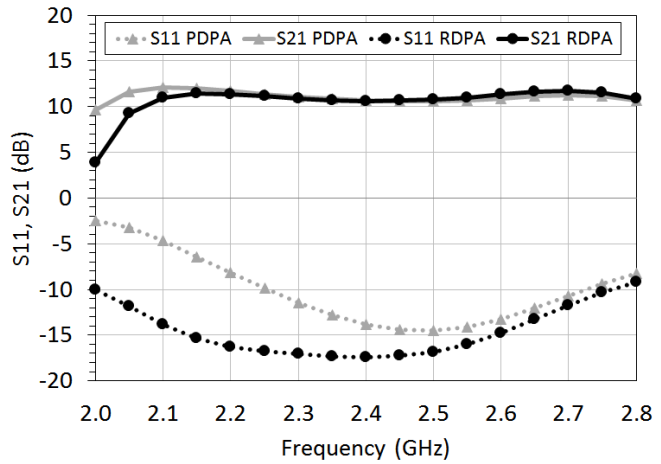

Fig. 12. Simulated input reflection coefficient (S_{11}) and small-signal gain (S_{21}) with $V_{gM} = -3.15$ V, $V_{gA} = -7$ V and $V_{dc} = 28$ V.

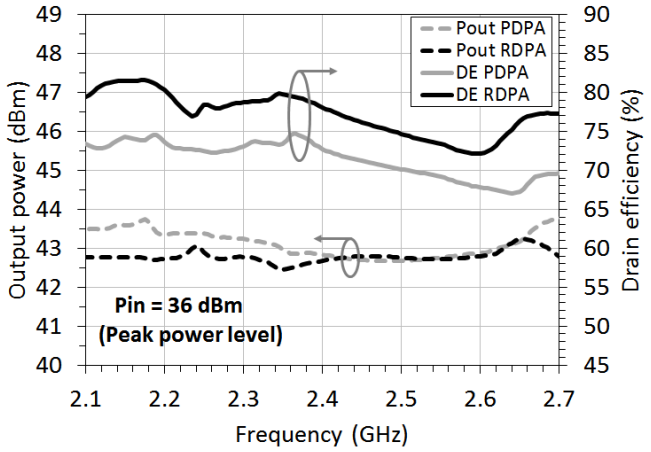

Fig. 13. Simulated output power and DE at PP with $V_{gM} = -3.15$ V, $V_{gA} = -7$ V and $V_{dc} = 28$ V.

power at the center frequencies of the lower and upper frequency bands. For the lower band, a maximum DE of 70% and 63% was achieved at PP and 6-dB BOP levels, respectively. For the upper band, the maximum DE was 63% at 40.5-dB output power. This performance could potentially be enhanced by improving the output matching and providing a better termination for the second harmonic. In Fig. 24, gain and DE were measured against output power at several frequencies across the bandwidth where we observe that lower frequencies (2.2–2.4 GHz) have better DE than the upper ones.

VI. Measurements with Modulated Signals

A. Robust PA linearity testing platform

In order to properly evaluate performance of the Reduced-α DPA, we have created a flexible testing platform as shown in

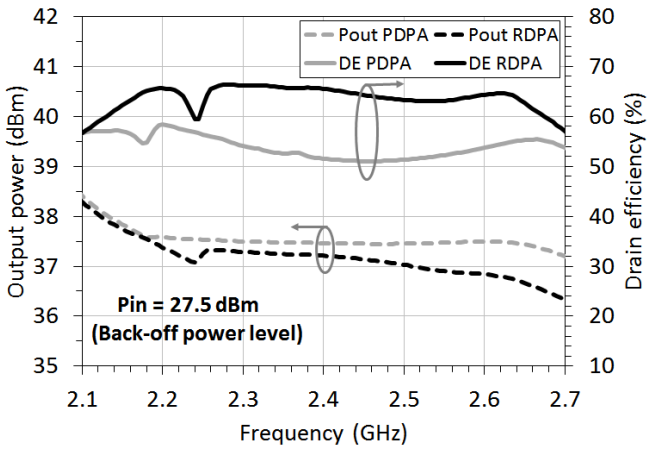

Fig. 14. Simulated output power and DE at BOP with $V_{gM} = -3.15$ V, $V_{gA} = -7$ V and $V_{dc} = 28$ V.

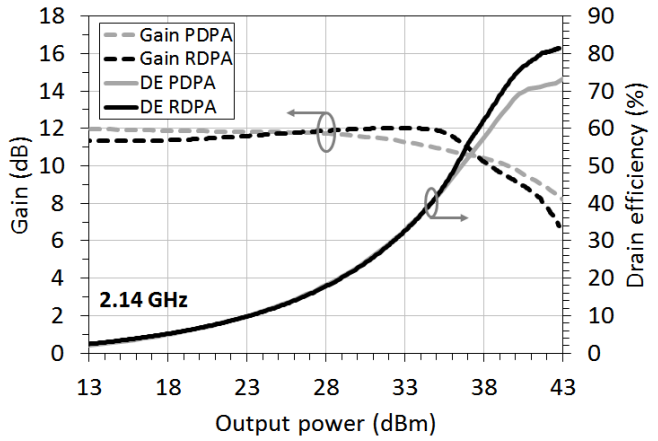

Fig. 15. Simulated gain and DE versus output power at 2.14 GHz with input power swept from 0 to 36 dBm with $V_{gM} = -3.15$ V, $V_{gA} = -7$ V and $V_{dc} = 28$ V.

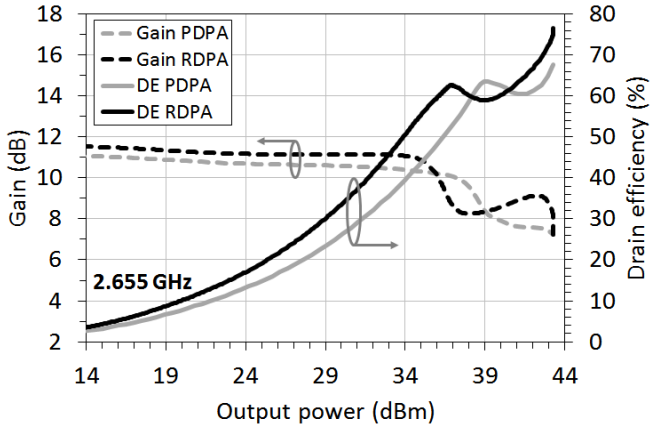

Fig. 16. Simulated gain and DE versus output power at 2.655 GHz with input power swept from 0 to 36 dBm with $V_{gM} = -3.15$ V, $V_{gA} = -7$ V and $V_{dc} = 28$ V.

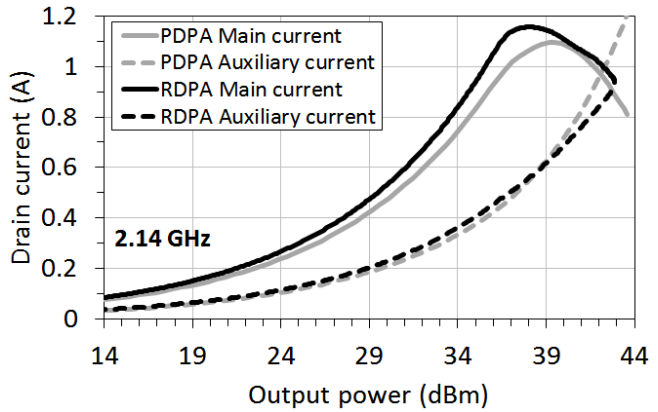

Fig. 17. Simulated Main and Auxiliary PAs drain currents (fundamental amplitudes) versus output power at 2.14 GHz with input power swept from 0 to 36 dBm with $V_{gM} = -3.15$ V, $V_{gA} = -7$ V and $V_{dc} = 28$ V.

Fig. 25, where includes a PC, an up-convertor, a device under test (DUT) and a spectrum analyzer. The PC with MATLAB was utilized for generating original baseband multicarrier wideband CDMA or/and LTE signals and performing digital up-conversion (DUC), then converted to digital IF by complex direct digital synthesizer (DDS). Depending on the testing purpose, an intraband carrier aggregation function is carried out in the digital domain. Moreover, modern modulated signals,

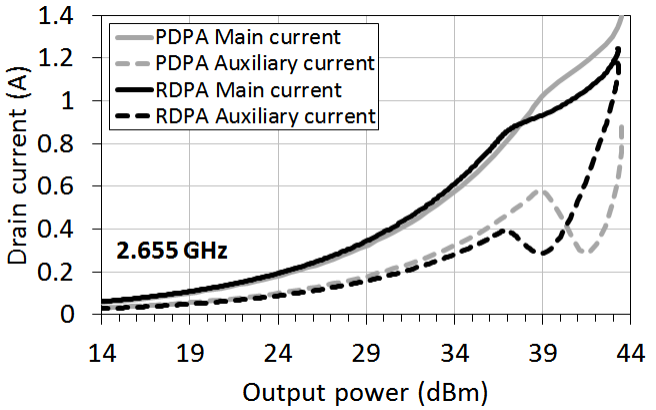

Fig. 18. Simulated Main and Auxiliary PAs drain currents (fundamental amplitudes) versus output power at 2.655 GHz with input power swept from 0 to 36 dBm with $V_{gM} = -3.15$ V, $V_{gA} = -7$ V and $V_{dc} = 28$ V.

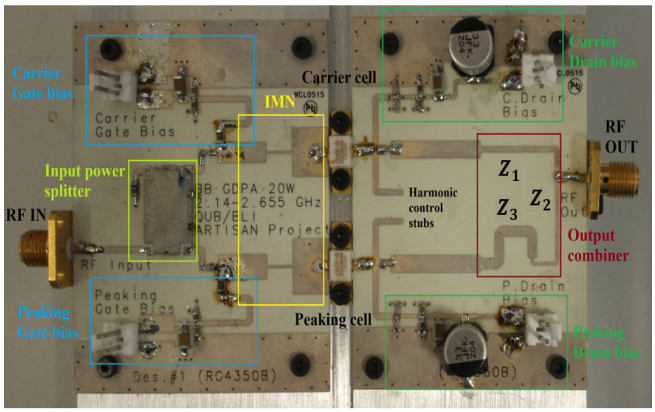

Fig. 19. Fabricated circuit prototype of the proposed Reduced-α DPA, measures 10 cm × 6.2 cm.

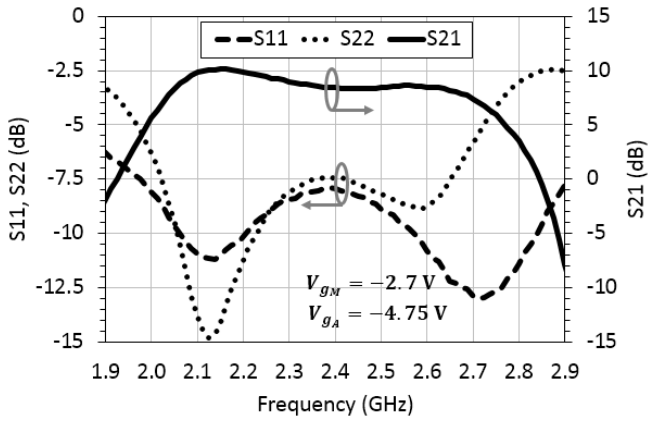

Fig. 20. Measured S-parameters with $V_{gM} = -2.7$ V, $V_{gA} = -4.75$ V and $V_{dc} = 28$ V.

especially LTE signals based on orthogonal frequency-division multiplexing (OFDM) technique, usually have a high peak-to-average power ratio (PAPR) value, which causes a lower efficiency of the PA in the back-off operation mode.

To remove the high peaks, we employed a crest factor reduction (CFR) function in the system, which has been largely accepted as one of the fundamental functions in 4G and fifth-generation (5G) wireless transceivers. Then, the processed modulated digital signals with 122.88 MSPS sampling rate were up-converted to the required RF frequencies to stimulate the DUT (the DPA), and are finally captured by the spectrum analyzer.

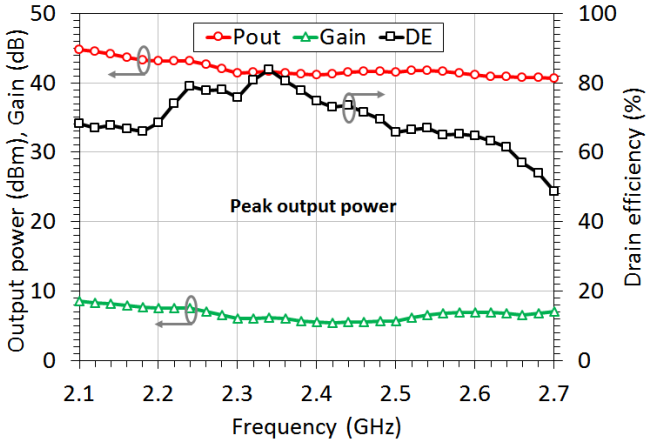

Fig. 21. Measured output power, gain and DE versus frequency at PP level with $V_{gM} = -2.7$ V, $V_{gA} = -4.75$ V and $V_{dc} = 28$ V.

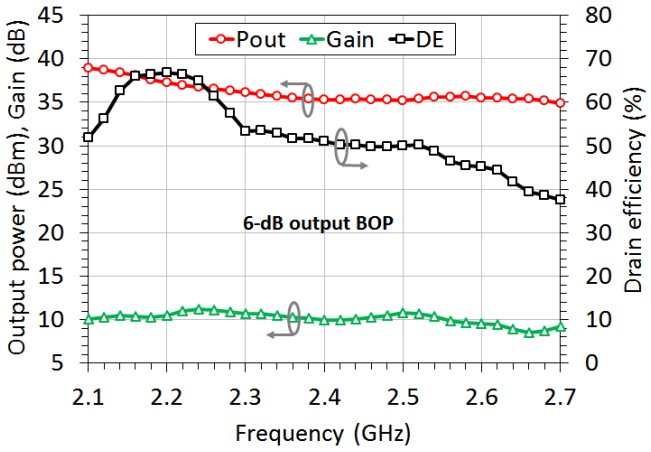

Fig. 22. Measured output power, gain and DE versus frequency at 6-dB output BOP level with $V_{gM} = -2.7$ V, $V_{gA} = -4.75$ V and $V_{dc} = 28$ V.

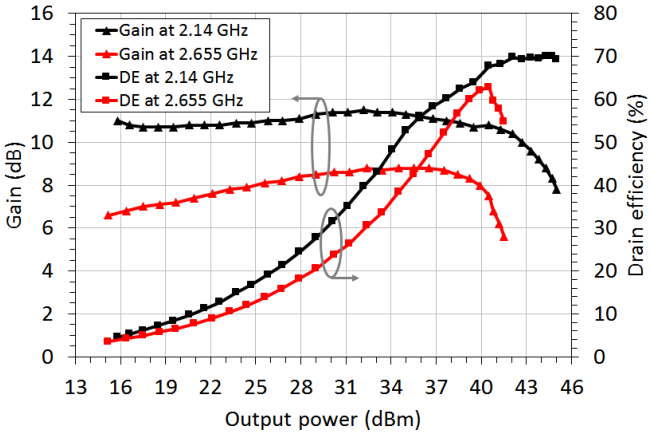

Fig. 23. Measured gain and DE versus output power at center frequencies of lower and upper bands with $V_{gM} = -2.7$ V, $V_{gA} = -4.75$ V and $V_{dc} = 28$ V.

B. DPA performance stimulated by modulated signals

For the purpose of evaluating the proposed DPA regarding linearity in the broadband and multiband applications, we created three different testing scenarios, i.e., the Reduced-α DPA was stimulated by three different types of modulated signals specified as shown in Table III. Specifically, scenario 1 depicts a traditional PA test using a single-carrier wideband

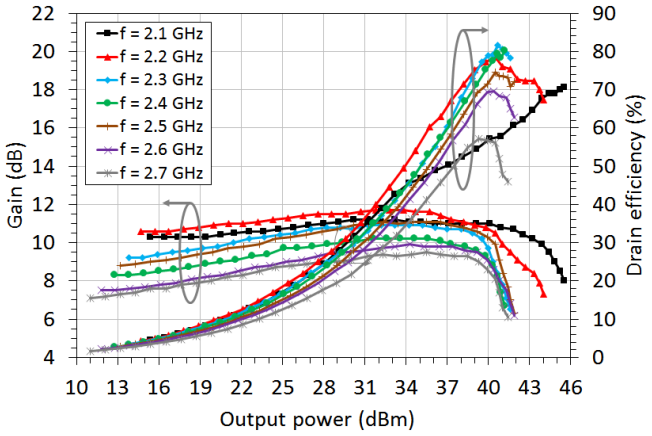

Fig. 24. Measured gain and DE versus output power at several frequencies with 100-MHz separations within 2.1–2.7 GHz frequency range, with $V_{gM} = -2.7$ V, $V_{gA} = -4.75$ V and $V_{dc} = 28$ V.

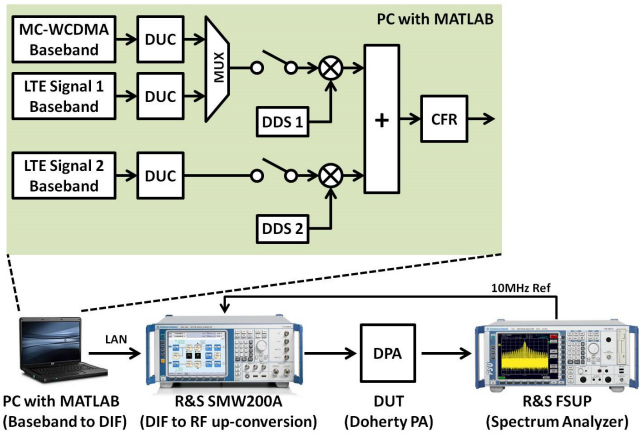

Fig. 25. Robust PA linearity evaluation platform.

TABLE III
DPA LINEARITY TESTING SCENARIOS

	Branch 1		Branch 2		Total PAPR (dB)	RF Frequency (GHz)
	Signal Type	Bandwidth (MHz)	Signal Type	Bandwidth (MHz)		
1	W-CDMA	5	-	-	6.5	2.14
2	LTE	20	-	-	7.5	2.655
3	LTE	10	LTE	10	8.0	2.655

CDMA (W-CDMA) signal (5-MHz bandwidth) as stimulation of the DPA. After the CFR function, the testing signal has a 6.5-dB PAPR value and is up-converted to Band 1, i.e., 2.14 GHz. Scenario 2 utilizes a 20-MHz LTE signal with a 7.5-dB PAPR value to excite the DPA at 2.655 GHz. Those two tests are used to illustrate the DPA performance regarding wideband signals applications. Furthermore, we provided another type of test to illustrate the DPA linearity performance regarding concurrent multiband wireless applications. For example, scenario 3 uses an intraband carrier aggregated signal [43] with an 8-dB PAPR value containing two LTE signals (10-MHz bandwidth each) and a 30-MHz gap in between (center RF frequency at 2.655 GHz).

Figs. 26 and 27 show the measured adjacent channel leakage ratios (ACLRs) and DE for scenario 1, where a maximum DE of 48% with $\text{ACLR}_1 = -25$ dBc and $\text{ACLR}_2 = -44.5$ dBc is obtained at average output power of 38.7 dBm. In the other

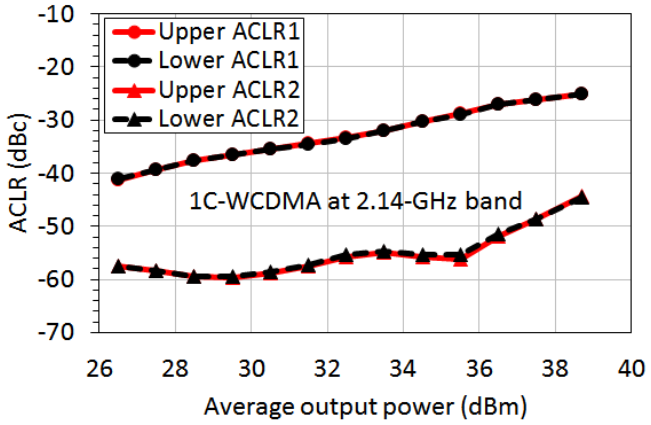

Fig. 26. Measured ACLRs against the average output power with single carrier 5-MHz W-CDMA signal at 2.14 GHz with 6.5-dB PAPR. $ACLR_1$ and $ACLR_2$ are at 5- and 10-MHz offsets from the carrier frequency, respectively.

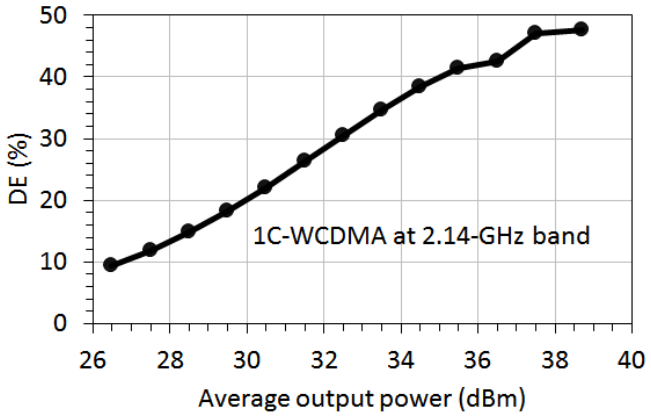

Fig. 27. Measured DE against the average output power with single carrier 5-MHz W-CDMA signal at 2.14 GHz with 6.5-dB PAPR.

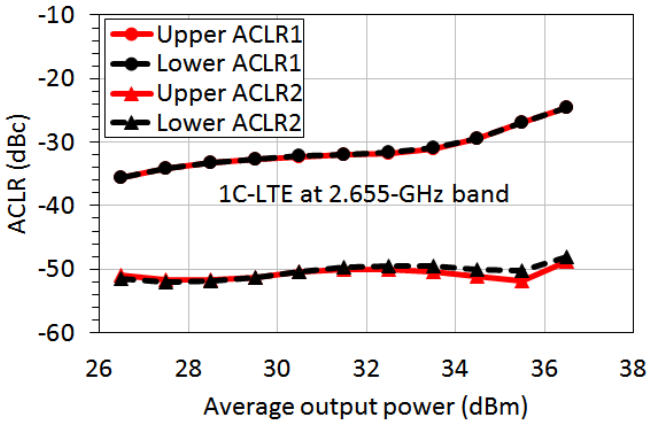

Fig. 28. Measured ACLRs against the average output power with single carrier 20-MHz LTE signal at 2.655 GHz with 7.5-dB PAPR. $ACLR_1$ and $ACLR_2$ are at 20- and 40-MHz offsets from the carrier frequency, respectively.

band (2.655 GHz) the DPA shows an $ACLR_1 = -24.5$ dBc and $ACLR_2 = -48.1$ dBc at an average output power of 36.5 dBm as depicted in Fig. 28. For the carrier aggregated signal scenario, $ACLR_1$, and $ACLR_2$ were found to be around –25.9 dBc and –48.6 dBc respectively as shown in Fig. 29.

Without any linearization approaches, the designed DPA delivered a reasonably good linearity performance over a wide bandwidth. In order to achieve a better linearity performance in the high efficiency saturated region, the linearization of the

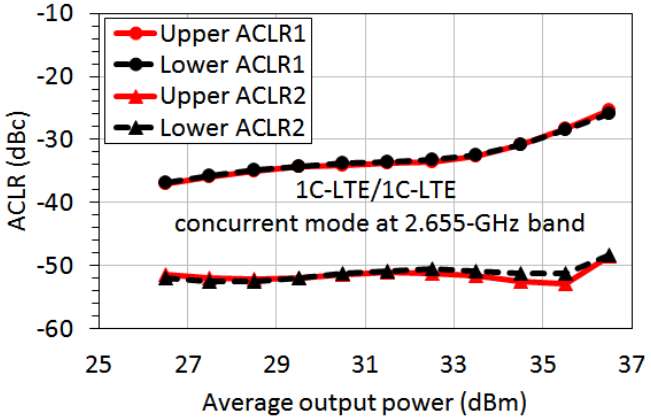

Fig. 29. Measured ACLRs against the average output power with intraband carrier aggregated signal contains two 10-MHz LTE signals separated by 30-MHz offset and centered around 2.655 GHz.

TABLE IV
COMPARISONS WITH OTHER PUBLISHED WIDEBAND GAN HEMTS DPAS

Ref.	Frequency (GHz)	P_{SAT} (dBm)	Peak power		6-dB BOP		Max. ACLR at BOP* (dBc)
			Max./Min. DE (%)	Bandwidth @ DE≥65% (MHz)	Max./Min. DE (%)	Bandwidth @ DE≥50% (MHz)	
[29]	1.05-2.55	42	83/45	550	58/35	220	−25
[25]	1.5-2.5	42	67/52	200	62/43	900	-
[24]	1.7-2.25	48.2-49.6	77/65	500	62/53	570	−30
[32]	1.7-2.3	53	72/58	250	61/41	240	−35
[31]	1.7-2.4	41	72/53	200	59/43	140	−30
[4]	1.7-2.6	42.1-45.3	55/50	0	55/41	200	−35
[30]	1.85-2.45	43	75/59	445	64/47	570	−23.5
[5]	1.96-2.46	42.2-44.2	66/52	80	53/40	110	−24
[33]	2.2-3.0	40.2-41.2	68/52	200	53/30	170	−30
[34]	3.0-3.6	43-44	65/56	0	54/38	360	-
This work	**2.1-2.66**	**43**	**84/57**	**500**	**67/39**	**420**	**−25**

* BOP is around 5-7 dB with different modulated signals used. Maximum value across the bandwidth is reported here.

DPA will be required for wireless applications. Due to its simple architecture and satisfactory performance, digital pre-distortion (DPD) [37] has been largely accepted as one of the fundamental blocks of wireless RF transceivers. In particular, the accurate PA behavior models proposed in [45]–[46] and effective wideband DPD verification approaches [47]–[48] have been successfully utilized for DPA linearization. However, due to the length restrictions, the linearization of the DPAs is beyond the scope of this paper.

In Table IV, the performance of the proposed DPA is summarized and compared with other wideband DPAs in the literature. Given two DE thresholds across the bandwidth (65% at PP and 50% at BOP) the Reduced-α DPA offers the highest maximum efficiencies at both PP and BOP levels, along with a balanced wideband performance where the DE is maintained above these thresholds for most of the intended bandwidth.

VII. Conclusion

A new theoretical approach that generalizes the conventional DPA theory is introduced in this paper. The approach introduces a theoretical parameter at the output combiner side which relates the combiner parameters through closed form formulae, and relaxes the Doherty operational conditions, thereby providing greater design flexibility. Based on the analysis, a new DPA design is proposed to enhance the performance of the parallel DPA published previously. Simulation results over 25% FBW have shown an improvement in the DE, reaching a maximum of 82% and 66% at peak and 6-dB BOP levels, respectively. The design was realized using GaN HEMTs to operate within 2.1–2.7 GHz frequency range. The measurements have shown a well-balanced wideband performance, where the DE was over 65% and 50% within most of the examined bandwidth at PP and 6-dB output BOP levels, respectively. The realized DPA has shown a reasonable linearity performance when measured with different modulated signals, where $ACLR_1$ was around –25 dBc. This paper supports broadband DPA development for modern wireless communication standards, and provides new concepts for the DPA output combining network design.

Acknowledgment

The authors wish to thank Dr. F. Pivit, R. Kearney, O. Burns (Bell Labs, Nokia Ireland), J. Knox and G. Rafferty (the Queen's University of Belfast) for their helpful technical discussions and contributions in this work.

References

[1] W. H. Doherty, "A new high efficiency power amplifier for modulated waves," in *Proc. IRE* , vol. 24, no. 9, pp. 1163–1182, Sep. 1936.

[2] S. C. Cripps, *RF Power amplifiers for wireless communications*. Norwood, MA, USA: Artech House, 2006.

[3] R. J. McMorrow, D. M. Upton and P. R. Maloney, "The microwave Doherty amplifier," in *IEEE MTT-S Int. Microw. Symp. Dig.*, 1994, pp. 1653–1656.

[4] K. Bathich, A. Z. Markos, and G. Boeck, "Frequency response analysis and bandwidth extension of the Doherty amplifier," *IEEE Trans. Microw. Theory Techn.*, vol. 59, no. 4, pp. 934–944, Apr. 2011.

[5] R. Darraji, F. M. Ghannouchi, and M. Helaoui, "Mitigation of bandwidth limitation in wireless Doherty amplifiers with substantial bandwidth enhancement using digital techniques," *IEEE Trans. Microw. Theory Techn.*, vol. 60, no. 9, pp. 2875–2885, Sep. 2012.

[6] K. Rawat, and F. M. Ghannouchi, "Design methodology for dual-band Doherty power amplifier with performance enhancement using dual-band offset lines," *IEEE Trans. Ind. Electron*., vol. 59, no. 12, pp. 4831–4842, Dec. 2012.

[7] J. Park, J. Yook, Y. Kim, and C. H. Lee, "Dual-band switching Doherty power amplifier using phase shifter composed of PIN diode," in *Eur. Microw. Integr. Circuits Conf.*, 2011, pp. 300–303.

[8] X. Li, W. Chen, Z. Feng, and F. M. Ghannouchi, "Design of dual-band tri-way GaN Doherty power amplifier with frequency dependent power division," *Electronics Letters*, vol. 48, no. 13, pp. 797–798, Jun. 2012.

[9] X. Li, W. Chen, Z. Lu, Z. Feng, Y. Chen, and F. M. Ghannouchi, "Design of dual-band multi-way Doherty power amplifiers," in *IEEE MTT-S Int. Microw. Symp. Dig*., 2012, pp. 1–3.

[10] P. Colantonio, F. Feudo, F. Giannini, R. Giofre, and L. Piazzon, "Design of a dual-band GaN Doherty amplifier," in *Microw. Radar and Wireless Commun. Int. Conf.*, 2010, pp. 1–4.

[11] P. Saad, P. Colantonio, L. Piazzon, F. Giannini, K. Andersson, and C. Fager, "Design of a concurrent dual-band 1.8–2.4-GHz GaN-HEMT Doherty power amplifier," *IEEE Trans. Microw. Theory Techn.*, vol. 60, no. 6, pp. 1840–1849, Jun. 2012.

[12] F. Taghian, A. Abdipour, A. Mohammadi, and P. M. Roodaki, "Design and nonlinear analysis of a dual-band Doherty power amplifier for ISM and LMDS applications," in *IEEE Appl. Electromagn. Conf*., 2011, pp. 1–4.

[13] K. Bathich, D. Gruner, and G. Boeck, "Analysis and design of dual-band GaN HEMT based Doherty amplifier," in *Eur. Microw. Integr. Circuits Conf.*, 2011, pp. 248–251.

[14] M. Hayakawa, K. Shiikuma, and T. Kaneko, "A total bandwidth expanded dual-band GaN Doherty PA toward the LTE-A carrier aggregation application," in *IEEE Compound Semicond. Integr. Circuit Symp. Dig*., 2013, pp. 1–4.

[15] W. Chen, S. Zhang; Y. Liu, Y. Liu, and F. M. Ghannouchi, "A concurrent dual-band uneven Doherty power amplifier with frequency-dependent input power division," *IEEE Trans. Circuits Syst. I, Reg. Papers*, vol. 61, no. 2, pp. 552–561, Feb. 2014.

[16] X. Li, W. Chen, Z. Zhang, Z. Feng, X. Tang, and K. Mouthaan, "A concurrent dual-band Doherty power amplifier," in *Asia-Pacific Microw. Conf.*, 2010, pp. 654–657.

[17] P. Saad, L. Piazzon, P. Colantonio, J. Moon, F. Giannini, K. Andersson, K. Bumman, and C. Fager, "Multi-band/multi-mode and efficient transmitter based on a Doherty power amplifier," in *Eur. Microw. Conf.*, 2012, pp. 1031–1034.

[18] W. Chen, S. A. Bassam, X. Li, Y. Liu, K. Rawat, M. Helaoui, F. M. Ghannouchi, and Z. Feng, "Design and linearization of concurrent dual-band Doherty power amplifier with frequency-dependent power ranges," *IEEE Trans. Microw. Theory Techn.*, vol. 59, no. 10, pp. 2537–2546, Oct. 2011.

[19] X. A. Nghiem, and R. Negra, "Design of a concurrent quad-band GaN-HEMT Doherty power amplifier for wireless applications," in *IEEE MTT-S Int. Microw. Symp. Dig.*, 2013, pp. 1–4.

[20] X. A. Nghiem, J. Guan, T. Hone, and R. Negra, "Design of concurrent multiband Doherty power amplifiers for wireless applications," *IEEE Trans. Microw. Theory Techn.*, vol. 61, no. 12, pp. 4559–4568, Dec. 2013.

[21] X. A. Nghiem, and R. Negra, "Novel design of a concurrent dual band GaN-HEMT Doherty power amplifier," in *Asia-Pacific Microw. Conf.*, 2012, pp. 364–366.

[22] AM. M. Mohamed, S. Boumaiza, and R. R. Mansour, "Electronically tunable Doherty power amplifier for multi-mode multi-band base stations," *IEEE Trans. Circuits Syst. I, Reg. Papers*, vol. 61, no. 4, pp. 1229–1240, Apr. 2014.

[23] AM. M. Mohamed, S. Boumaiza, and R. R. Mansour, "Reconfigurable Doherty power amplifier for multifrequency wireless radio systems," *IEEE Trans. Microw. Theory Techn.*, vol. 61, no. 4, pp. 1588–1598, Apr. 2013.

[24] K. Bathich, and G. Boeck, "Wideband harmonically-tuned GaN Doherty power amplifier," in *IEEE MTT-S Int. Microw. Symp. Dig*., 2012, pp. 1–3.

[25] D. Gustafsson, C. M. Andersson, and C. Fager, "A modified Doherty power amplifier with extended bandwidth and reconfigurable efficiency," *IEEE Trans. Microw. Theory Techn.*, vol. 61, no. 1, pp. 533–542, Jan. 2013.

[26] A. Grebennikov, and J. Wong, "A dual-band parallel Doherty power amplifier for wireless applications," *IEEE Trans. Microw. Theory Techn.*, vol. 60, no. 10, pp. 3214–3222, Oct. 2012.

[27] R. Giofre, L. Piazzon, P. Colantonio, and F. Giannini, "A distributed matching/combining network suitable for Doherty power amplifiers covering more than an octave frequency band," in *IEEE MTT-S Int. Microw. Symp. Dig.*, 2014, pp. 1–3.

[28] D.Y.-T. Wu, J. Annes, M. Bokatius, P. Hart, E. Krvavac, and G. Tucker, "A 350 W, 790 to 960 MHz wideband LDMOS Doherty amplifier using a modified combining scheme," in *IEEE MTT-S Int. Microw. Symp. Dig.*, 2014, pp.1–4.

[29] R. Giofre, L. Piazzon, P. Colantonio, and F. Giannini, "A closed-form design technique for ultra-wideband Doherty power amplifiers," *IEEE Trans. Microw. Theory Techn.*, vol. 62, no. 12, pp. 3414–3424, Dec. 2014.

[30] X. A. Nghiem, J. Guan, and R. Negra, "Design of a broadband three-way sequential Doherty power amplifier for modern wireless communications," in *IEEE MTT-S Int. Microw. Symp. Dig*., 2014, pp. 1–4.

[31] L. Piazzon, R. Giofre, P. Colantonio, and F. Giannini, "A wideband Doherty architecture with 36% of fractional bandwidth," *IEEE Microw. Wireless Compon. Lett.*, vol. 23, no. 11, pp. 626–628, Nov. 2013.

[32] K. Bathich, M. T. Arnous, and G. Boeck, "Design of 200 W wideband Doherty amplifier with 34 % bandwidth," in *Eur. Microw. Conf*., 2013, pp. 279–282.

[33] G. Sun, and R. H. Jansen, "Broadband Doherty power amplifier via real frequency technique," *IEEE Trans. Microw. Theory Techn.*, vol. 60, no. 1, pp. 99–111, Jan. 2012.

[34] J. M. Rubio, J. Fang, V. Camarchia, R. Quaglia, M. Pirola, G. Ghione, "3–3.6-GHz wideband GaN Doherty power amplifier exploiting output

compensation stages," *IEEE Trans. Microw. Theory Techn.*, vol. 60, no. 8, pp. 2543–2548, Aug. 2012.
[35] J. Son, I. Kim, J. Moon, J. Lee, and B. Kim, "A highly efficient asymmetric Doherty Power Amplifier with a new output combining circuit," in *Proc. IEEE Int. Microw., Commun., Antennas Electron. Syst. Conf.*, 2011, pp.1–4.
[36] S. Chen, and Q. Xue, "Optimized load modulation network for Doherty power amplifier performance enhancement," *IEEE Trans. Microw. Theory Techn*, vol. 60, no. 11, pp. 3474–3481, Nov. 2012.
[37] J. Xia, X. Zhu, L. Zhang, J. Zhai, and Y. Sun, "High-efficiency GaN Doherty power amplifier for 100-MHz LTE-Advanced application based on modified load modulation network," *IEEE Trans. Microw. Theory Techn*, vol. 61, no. 8, pp. 2911–2921, Aug. 2013.
[38] A. Barakat, M. Thian, V. Fusco, "Towards generalized Doherty power amplifier design for wideband multimode operation," in *SBMO/IEEE MTT-S Int. Microw. Optoelectronics Conf.*, 2015, pp.1–5.
[39] D. M. Pozar, *Microwave Engineering*, 2nd ed. New York: Wiley, 1998, pp. 271–275.
[40] N. O. Sokal and A. D. Sokal, "Class-E: A new class of high-efficiency tuned single ended switching power amplifiers," *IEEE J. Solid-State Circuits*, vol. SC-10, pp. 168–176, Jun. 1975.
[41] M. Thian and V. Fusco, "Series-L/parallel-tuned comparison with shunt-C/series-tuned class-E power amplifier," *IEE Circuits Devices Syst.*, vol. 152, no. 6, pp. 709–717, Dec. 2005.
[42] M. Thian and V. Fusco, "Exploring figures of merit associated with the suboptimum operation of class-E power amplifiers," *IET Circuits Devices Syst.*, vol. 1, no. 6, pp. 401–407, Dec. 2007.
[43] E-UTRA User Equipment (UE) radio transmission and reception, 3GPP Standard TS 36.101, V13.2, 2014.
[44] L. Guan and A. Zhu, "Green communications: Digital predistortion for wideband RF power amplifiers", *IEEE Microw. Mag.*, vol. 15, no. 7, pp.84-99,2014.
[45] D. R. Morgan, Z. Ma, J. Kim, M. G. Zierdt, and J. Pastalan, "A generalized memory polynomial model for digital predistortion of RF power amplifiers," *IEEE Trans. Signal Processing*, vol. 54, no. 10, pp. 3852–3860, 2006.
[46] A. Zhu, "Decomposed vector rotation-based behavioral modeling for digital predistortion of RF power amplifiers," *IEEE Trans. Microw. Theory Techn*, vol. 63, no 02, pp. 737-744, Feb. 2015.
[47] L. Guan, R. Kearney, C. Yu, and A. Zhu, "High-performance digital predistortion test platform development for wideband RF power amplifiers," *Int. J. Microw. Wireless Technol.*, vol. 5, no. 02, pp. 149–162, Apr. 2013.
[48] C. Yu, L. Guan, E. Zhu, and A. Zhu, "Band-limited Volterra Series-based digital predistortion for wideband RF power amplifiers," *IEEE Trans. Microw. Theory Techn*, vol. 60, no.12, pp. 4198-4208, Dec 2012.

Ayman Barakat (S'14) received the B.Sc. degree in electrical engineering from Ain Shams University, Cairo, Egypt, in 2005, the M.Sc. degree in electrical engineering from Tampere University of Technology, Tampere, Finland, in 2013, and is currently working toward the Ph.D. degree in electrical engineering at the Queen's University of Belfast, Belfast, U.K.

From March 2006 to July 2011, he worked within the telecommunication and electrical industry. He is currently an Early Stage Researcher with the Queen's University of Belfast. His research interests include switched-mode and Doherty power amplifier design for multiband transmitters.

Mury Thian obtained the B.Sc. degree from Atma Jaya Catholic University, Jakarta, Indonesia, the M.Sc. degree from Delft University of Technology, Delft, the Netherlands, and the Ph.D. degree from the Queen's University of Belfast, Belfast, United Kingdom, all in electronics engineering.

He was with Astra International ISUZU (Jakarta, Indonesia), NXP Semiconductors (Nijmegen, the Netherlands), the University of Birmingham (Birmingham, United Kingdom), and Infineon Technologies (Villach, Austria) before joining the Queen's University of Belfast (Belfast, United Kingdom) as a lecturer in 2013.

Dr. Thian has published over 45 journal and conference paper and two book chapters. He has served as a TPC member for IEEE Radio Wireless Week PAWR. He has been invited to chair sessions and give talks in a number of IEEE major conferences and workshops. He was a Marie Curie Fellow and the 2008 finalist of the British Association for the Advancement of Science.

Vincent Fusco PhD, DSc, IEEE Fellow, FREng, FIET, FIAE, FRIA. In 2012 he was awarded the IET senior achievement award the Mountbatten Medal for seminal contributions in the field of microwave electronics and its impact on UK industry.

His fundamental work on active antenna front-end techniques has provided generic advances in low cost phased and self-tracking antenna array architectures. This work has strongly impacted advanced system concepts in areas requiring communications between un-stabilized platforms and is enabling the next generation of mobile terrestrial to satellite broadband internet connectivity. He has written over 450 papers and two books and holds a number of antenna related patents. He co-founded a major research institute in electronics and information technology (ECIT) at Queens University Belfast which now employs 170 people where he is currently its chief technology officer.

Senad Bulja (M'07–SM'12) received the B.Eng. (with distinction) and Ph.D. degrees from the University of Essex, Colchester, U.K., in 2002 and 2007, respectively.

From 2007 to 2010, he was a Senior Research Officer with the School of Computer Science and Electronic Engineering, University of Essex, where he was involved with the characterization of liquid crystals at microwave and millimeter-wave frequencies, and development of liquid-crystal-based millimeter-wave devices. In 2010, he joined Bell Labs, Dublin, Ireland, where he is currently a Member of Technical Staff. He authored or coauthored over 30 papers in international journals and conference proceedings and holds over 30 patents. His research interests include variable microwave devices, microwave amplifier linearization techniques, memory effects description in RF transistors, characterization of liquid crystals at microwave and millimeter-wave frequencies, and more recently, microwave filters.

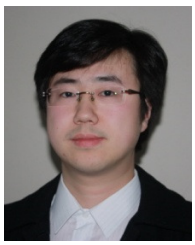

Lei Guan (S'09 – M'12) received the B.E. and the M.E. degree from Harbin Institute of Technology (HIT), Harbin, China in 2006 and 2008, respectively and Ph.D. degree in electronic engineering from University College Dublin (UCD), Dublin, Ireland, in 2012.

He then spent two years involved with industrial-related research projects with UCD and Trinity College Dublin, respectively. He is currently a Member of Technical Staff with Nokia Bell Labs, Dublin, Ireland. He possesses ten years of R&D experience in field-programmable gate arrays (FPGAs) and digital signal processing. His research interests include RF signal conditioning algorithms for digitally assisted high-efficient RF front-ends such as digital predistortion (DPD) and crest factor reduction (CFR), nonlinear system identification, software-defined radio systems, and wideband RF front-ends. He also has strong interests in high-performance computing platforms like FPGAs and all programmable systems-on-chip (SoCs), and their potentials in next-generation wireless systems, hybrid beamforming antenna array systems, large scale antenna systems, and cloud radio access networks.